

Ultrasound-CT Registration in Image-Guided Pedicle Screw Placement

João Filipe Fernandes Mocho Ferreira¹

Instituto Superior Técnico, Lisbon, Portugal
¹e-mail: joao.f.mocho.ferreira@tecnico.ulisboa.pt

ABSTRACT

Pedicle screws placement is among the most performed procedures for treating chronic lower back pain and increasing the accuracy of their insertion is crucial. Image-guided surgery is one of the most advanced techniques for inserting pedicle screws in the lumbar spine, presenting better results than traditional approaches. Despite of this accuracy improvement, most image-guided procedures use ionizing radiation for acquiring intraoperative images, which led to studies aimed at substituting the intraoperative imaging by a low cost, real-time and non-ionizing alternative, such as ultrasound imaging. The present project simulates all necessary steps for performing image-guided pedicle screw placement, using Free-hand 3-D Ultrasound as intraoperative imaging modality. For this, it was created a lumbar spine phantom, which was used as subject to perform a preoperative CT-scan, where segmentation and surgical planning was performed, and to acquire intraoperative US volumes, using an optical measurement system to track an US probe. The point clouds segmented from the CT and US data were then registered using an initial approximation based on fiducial identification and refined by the Iterative Closest Point algorithm, which allowed to compute transformation from the CT referential to the intraoperative coordinate system. A group of five US volumes were acquired from different regions of the phantom and were merged with the CT data, presenting a registration error around 2 mm. After combining the surgical plans and the registration results in a navigation system, it was concluded that, although presenting some limitations, ultrasound could be an alternative for intraoperative imaging in IG surgery.

Keywords: Lumbar Spine; Pedicle Screws; Phantom; Surgical Planning; Image-Guided Surgery; Intraoperative; Ultrasound; Point Cloud; Registration.

1. Introduction

Nowadays, lower back pain (LBP) is a condition with a great impact in general well-being and its prevalence has been increasing [1]. Although it can be caused by different diseases or accidents, chronic LBP is often caused by more complex conditions, such as intravertebral discs disorders or deformity. Patients suffering from chronic LBP showing no signs of improvement after nonsurgical procedures may be considered to a lumbar spine surgery [2]. Most lumbar spine surgeries performed worldwide, as nerve decompression, intervertebral fusion or deformity correction, use stabilization mechanisms to fixate the spine in its defined position, give support and prevent relative motion between different spine segments. This stabilization mechanisms are composed of pedicular screws and metallic rods.

Pedicle screws, shown in Figure 1, are considered the “state of the art” for the treatment of spine deformities [3]. They are placed through the pedicle region of the vertebrae by a posterior approach and allow to rigidly attach the metallic rods to the spine segments that the surgeon wants to stabilize, guiding the vertebrae to their new position or simply fixating them in their current location.



Figure 1 - Pedicle screw.

Since pedicle screws began to be used, the surgical procedures to insert them have been changing, based on the new techniques which have been developed, such as minimally invasive surgeries [4]–[6] and image guided procedures [7]. Image guided (IG) placement of pedicle screws (Figure 2) arise recently with the advent of powerful computer systems capable of real time tracking surgical instruments in conjunction with preoperative and intraoperative medical images. This technique allowed to increase the accuracy and security of the procedures with pedicle screws [8].

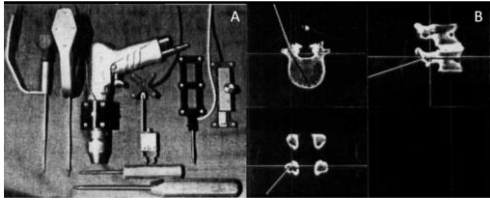


Figure 2 - Image guided surgery. A: Surgical tools with position tracked markers. B: Detail of the navigation system, with the CT plan and the intraoperative COS matched. (Adapted from [7])

In an IG surgery for inserting pedicle screws it is crucial to acquire some intraoperative volumetric images, that can be merged with the preoperative plans by registering the different imaging data and which must be concordant with the intraoperative referential or coordinate system (COS). The surgical instruments are also tracked in this intraoperative COS, allowing the surgeon to have real-time feedback of the positions of the tools in a navigation system. The more recent IG setups commercially available make use of 3-D fluoroscopy, CT or MRI to acquire their intraoperative images. Although this imaging modalities present good image quality and detail of the spine region, they present some disadvantages like the emission of ionizing radiation (except for MRI), their high cost and the reduced mobility. These factors led to studies aimed at replacing the currently used intraoperative imaging methods with a low-cost, mobile and non-ionizing alternative, such as Ultrasounds (US) [9], [10].

This work represents a step further for performing IG surgeries for placing pedicle screws using low cost, non-ionizing intraoperative imaging. For this project we acquired US volume data to obtain the location of the spine during surgery in the intraoperative referential, which after registration with the preoperative CT data, allowed to track the surgical tools relative to the same referential using a navigation system, assisting the surgeon to perform pedicle screw placement as planned in the preoperative data.

2. Objectives

The main objective of the proposed project was to simulate an image-guided surgery for inserting pedicle screws in the lumbar spine, using Freehand 3-D Ultrasound imaging as the intraoperative imaging modality and performing registration between the preoperative CT data with the surgical plans and the intraoperative data. To achieve this goal, we divided it in simpler objectives: (a) construction of a lumbar spine phantom, to perform the different preoperative stages of the surgery; (b) acquisition of preoperative CT data, to obtain the 3-D models of each vertebrae and perform the surgical plans; (c) acquisition of intraoperative Freehand 3-D Ultrasound volumes, to know the intraoperative position of the lumbar spine phantom in the surgical theatre; (d) registration of the pre and intraoperative data, to compute the pedicle screw plans, with their insertion points and orientations, in the surgical theatre referential; (e) development of a simple navigation system, to visualize in real-time the surgical tools

and their relative position to the lumbar spine model and the surgical plans.

3. Lumbar spine phantom

Before the implementation of any practical work in this project, it was necessary to create a testing subject, which consisted in a 3-D model of the lumbar region (T11-12 + L1-5 vertebrae), based on a real CT scan of an adult female.

We started by segmenting the CT of the patient manually in 3D Slicer (<http://www.slicer.org>), exporting the models and 3-D printing them in acrylonitrile butadiene styrene (ABS) using a MakerBot' The Replicator*. After printing, the vertebrae models were stacked using flexible silicone as their intervertebral discs and capsular ligaments. The complete model was placed in a plastic box and covered with a mixture of gelatine and glycerine, which presented density similar to human tissues, and provided a medium for acquiring images of the model. The final lumbar spine phantom is shown in Figure 3.



Figure 3 - Complete lumbar spine phantom.

4. Methods

Figure 4 shows the possible structure of an ultrasound image guided surgery for pedicle screw insertion. The patient starts by performing a CT scan from which a 3 D model of its lumbar spine is created. Then the physician determines the spine injury or disease, the affected vertebrae and plans the trajectory for the pedicle screws placement. Intraoperatively, the physician starts by acquiring the tracked ultrasound data, creating a new 3 D model of the lumbar spine based on the intraoperative US data. The two 3 D models, CT derived and US derived, are merged using a registration algorithm, allowing the navigation system to show the CT planned trajectories in the intraoperative coordinate system (COS).

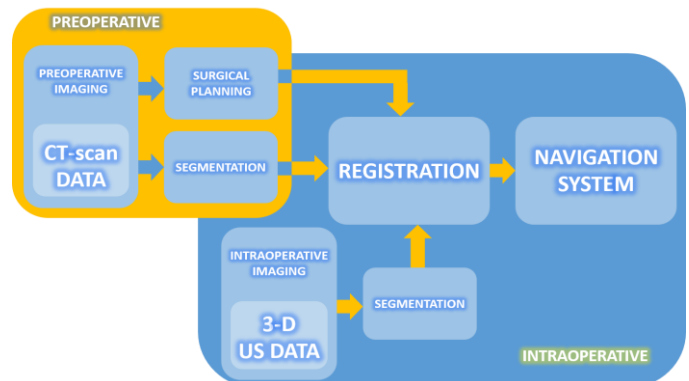


Figure 4 - Proposed structure of an US image guided surgery for pedicle screw placement.

CT-scan, CT model and surgical planning

The first step of our IG procedure was to perform a CT scan to the lumbar spine phantom at Hospital de Santa Maria, in a Philips Brilliance CT 64-slice (Koninklijke Philips N.V., Amsterdam, Netherlands). This CT scan was then exported in a Digital Imaging and Communications in Medicine (DICOM) format. The DICOM file contained a 768x768x266 3-D matrix, where each element corresponds to a voxel (a 3D pixel) with fixed height, weight and depth in *mm*. Along with the voxels, the DICOM file includes meta-data with useful information, such as the voxels sizes in mm, the distance between adjacent axial slices, the CT-scan coordinate system (COS), the date and time of the CT-scan and other information about the CT device and the CT-scan parameters. Figure 5 shows the computed tomography images, where it is possible to observe a good contrast between the different materials.

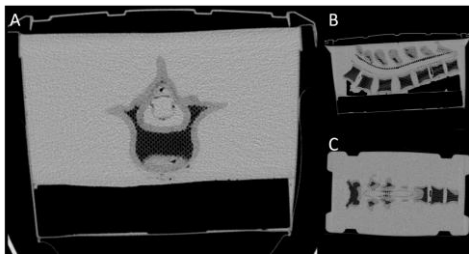


Figure 5 - CT scan of the Lumbar spine phantom: axial (A), sagittal (B) and coronal (C) slices.

The segmentation of the CT scan of the lumbar spine phantom was performed also in 3D Slicer but using a semi-automatic process with three steps: (a) applying an intensity threshold, (b) using the island tool and (c) manually finishing the segmentation, allowing a correct segmentation. The segmented models of the lumbar spine phantom were then exported, used to extract a Point Cloud to perform registration and were used to perform the surgical planning. Since the US waves can only reach the posterior regions of the lumbar spine, the CT-derived Point Cloud used in the registration process must include that same region. To identify these regions, we scanned the columns of each slice of the segmented CT, highlighting the first pixel of the segmentation, which correspond to the posteriormost portions.

To perform the surgical planning, a graphical user interface (GUI) was created in MATLAB®. This GUI allowed to open the DICOM files to visualize the CT data, load the vertebrae 3-D models and visualize them in the CT scan COS. Then, it allows to graphically choose the insertion point of the pedicle screw and its orientation while the user visualizes the intersections between the screws and the CT slices. The location and orientation of the pedicle screws were chosen according to medical orientation, with the insertion in a region slightly inferior to the intersection between the transverse process and the superior articular process, in the posterior projection of the pedicles. The orientation was chosen so that the screw passes through the pedicle as close as possible to its centre. For this work, we planned the insertion of pedicle screws in the L2, L3

and L4 vertebrae. These vertebrae were chosen because they present the closest shape to a typical lumbar vertebra.

Freehand 3-D Ultrasound imaging

The Freehand 3 D Ultrasound imaging, one of the key steps in this project, allows to compute a 3 D volume based on a US scan. This is possible by recording a large set of 2 D US frames while the US probe's location in the intraoperative COS is being tracked, allowing to match the US data with its corresponding position in the intraoperative space.

The devices used in this step were the Passive Polaris Spectra System (Northern Digital Incorporated, Waterloo, Ontario, Canada), a mobile system able to track the 3-D position and orientation of markers attached to surgical tools [11], with two tracked tools, namely a pointer and a tool rigidly attached to the US probe, the ProSound 2 Ultrasound System (Hitachi Aloka, Mitaka, Tokyo, Japan), connected to the UST 586 5 transducer of the same manufacturer and a computer running Stradwin (<http://mi.eng.cam.ac.uk/~rwp/stradwin>) [12], the software used to perform the calibration and the acquisition of the Freehand 3-D Ultrasound data.

Through the details presented in Figure 6, it is possible to understand all the different existing COS in the acquisition of the 3 D Ultrasound volumes in this project: the Polaris system COS (Polaris) which represents the intraoperative COS, the US probe COS (probeUS) and the US frame COS (frameUS) and all the transformations between each COS.

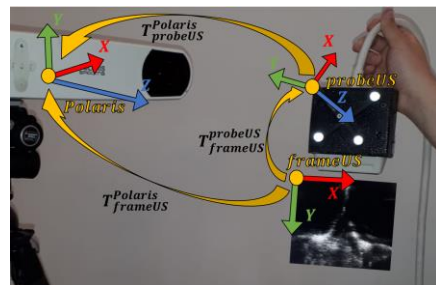


Figure 6 - Freehand 3 D Ultrasound existing COS and transformations between them.

To compute the 3-D US-derived volume it is imperative to know the intraoperative position of each pixel of an US image, in other words, it is necessary to know the transformation between the frameUS COS and the Polaris COS, $T_{frameUS}^{Polaris}$. Since the Polaris system can only track the tool attached to the probe and not the image acquired by it, $T_{frameUS}^{Polaris}$ is indirectly computed by

$$T_{frameUS}^{Polaris} = T_{probeUS}^{Polaris} * T_{frameUS}^{probeUS} \quad (1)$$

where $T_{probeUS}^{Polaris}$ is known by the Polaris system and $T_{frameUS}^{probeUS}$ must be calculated in a process known as Probe Calibration.

The usual approach to perform Probe Calibration is to scan a phantom, an object whose dimensions are known, that place constraints on the eight calibration parameters necessary to

fully define the transformation: two image scales (S_u and S_v , the x scale and y scale, respectively), three translations (tx , ty and tz , in the x, y and z directions, respectively, defining the translation vector $t_{frameUS}^{probeUS}$) and three rotations (α , β and γ , about the z, y and x axes, respectively, defining the rotation matrix $R_{frameUS}^{probeUS}$) [13].

The Stradwin software includes a Probe Calibration feature that uses the tip of the Polaris Pointer tool as a calibration phantom, avoiding the need of printing a complex phantom, while allowing good calibration.

Before starting the calibration process, and since the Polaris system can only track the pointer tool and not its tip, we needed also to compute the position of the tip in the pointer COS, performing a method called pointer pivoting. To perform this step, the tip must be pinned to a stationary point, while the pointer tool is rotated in a cone shape around the tip, in an angle between 30 and 60 degrees from the vertical axis. After several position acquisitions, Stradwin computes the offset of the pointer tip, by trying to calculate a point equidistant to all the pointer tool positions acquired by the Polaris system.

After the pivoting step, probe calibration could be performed. Figure 7 shows the device setup used in the probe calibration process, as well as the COS and transformations involved in this process. The US images in this task were acquired in a water bath with a known temperature, granting a material in which the US waves can propagate. Knowing the water's temperature allows Stradwin to make a necessary and automatic calibration correction, due to the differences in sound velocity in water at different temperatures.

During the probe calibration, we scanned a set of points p_i with the US system. Those points result from aligning the pointer's tip in the US plane, creating a bright spot in the US images, which are automatically segmented by Stradwin.

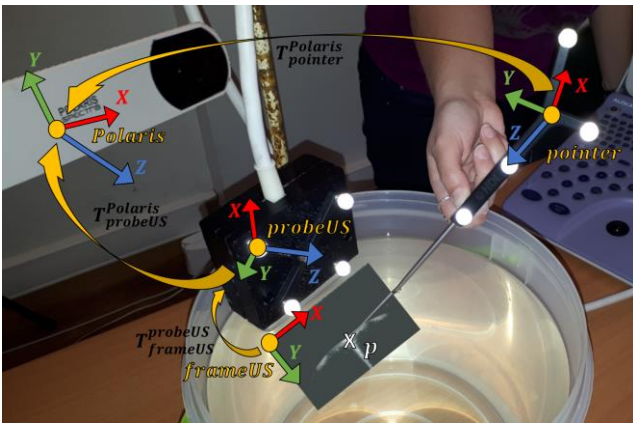


Figure 7 - Probe calibration. Detail of the existing COS and transformations between them.

This segmentation returns $p_i^{frameUS'} = (u_i, v_i, 0)$, where u_i and v_i are the column and row indices of each point p_i in the US frame. These points, in pixels, are converted to metric units by a scaling factor

$$T_{scale} = \begin{bmatrix} s_u & 0 & 0 \\ 0 & s_v & 0 \\ 0 & 0 & 0 \end{bmatrix} \quad (2)$$

where s_u and s_v are the scaling factors in millimeters per pixel, to compute the segmented points in the frameUS COS, $p_i^{frameUS'}$. These points can then be computed in the Polaris COS by

$$p_i^{Polaris} = T_{probeUS_i}^{Polaris} * T_{frameUS}^{probeUS} * T_{scale} * p_i^{frameUS'} \quad (3)$$

where $T_{probeUS_i}^{Polaris}$ is the transformation between the probeUS COS and Polaris COS at the moment of the acquisition of p_i and is given by the Polaris system, $p_i^{frameUS'}$ results from the automatic US image segmentation performed by the Stradwin software, and $T_{frameUS}^{probeUS}$ and T_{scale} are unknown.

In other hand, since the segmented points came from the pointer's tip, and therefore their 3-D location is the same, there is another way of computing them in the Polaris COS, which is given by

$$p_i^{Polaris} = T_{pointer_i}^{Polaris} * p_i^{pointer} \quad (4)$$

where $T_{pointer_i}^{Polaris}$ is the transformation between the pointer COS and Polaris COS at the moment of the acquisition of p_i and is given by the Polaris system and $p_i^{pointer}$ is the constant offset of the tip in the pointer COS and results from the pointer pivoting.

Equating (3) and (4), we get

$$\begin{aligned} & T_{pointer_i}^{Polaris} * p_i^{pointer} \\ &= T_{probeUS_i}^{Polaris} * T_{frameUS}^{probeUS} * T_{scale} * p_i^{frameUS'} \end{aligned} \quad (5)$$

which, after locating a minimum of three noncollinear p_i , allow to perform the probe calibration by minimizing

$$\min \sum_i \left| T_{probeUS_i}^{Polaris} * T_{frameUS}^{probeUS} * T_{scale} * p_i^{frameUS'} - T_{pointer_i}^{Polaris} * p_i^{pointer} \right| \quad (6)$$

where $||$ denotes the Euclidean norm of \mathbb{R}^3 . Stradwin automatically minimizes the previous equation using the iterative Levenberg-Marquardt algorithm, computing $T_{frameUS}^{probeUS}$ and T_{scale} [13], [14].

After performing Probe Calibration, we started the acquisitions by scanning the surface of our lumbar spine phantom. To ensure an efficient propagation of the US waves, we placed a conductor gel in the tip of the probe, eliminating the air between the probe and the phantom and decreasing the acoustic impedance. The conductor gel used was the Quick-Eco Gel® (LESSA - AB MEDICA GROUP, S.A., Barberà del Vallès, Barcelona, Spain).

A group of five US volumes were acquired in this project: three scans of the entire length of the phantom with the US probe acquiring axial frames, as shown in Figure 8, and two scans of the L3 vertebra with the US probe acquiring perpendicular to the axial plane and performing a slightly radial movement. The first scan was acquired medially, with the center of the US probe aligned with the vertebrae' spinous

processes. The second and third scans were acquired with the center of the US probe aligned with the left articular processes and right articular processes, respectively.



Figure 8 - Axial acquisitions of the entire length of the phantom: medially (A), left (B), right (C).

The two L3 scans were acquired in the right side of the vertebra. These single vertebra acquisitions were performed with the objective of performing registration using just one vertebral model, because although each vertebra is a single rigid body, they can suffer movements relative to each other, and this problem can only be overcome by registering a single vertebra.

All the US acquisitions were performed with the same US settings, an image depth of 50 mm, US waves of 7.5 MHz and a gain of 64.

Finishing each acquisition, the 3-D US data was saved. Stradwin allows to export the US frames and the information about the COS transformations in different formats, but the chosen ones were .JPEG, to save each US frame, and .SW, a Stradwin base format, which is essentially a text format with all the information regarding the calibration parameters, the number of frames recorded, the recording time or the transformations for each image.

The US-derived Point Clouds were created by segmenting the acquired US images. To perform it, another MATLAB® GUI was created. This GUI allowed to load the .SW file and each of the .JPEG US frames, to define the segmentation region of interest (ROI) and the initial and final frames. The segmentation was made in 4 steps: (a) Filtering with a median filter which reduces noise without distorting the contours of the vertebrae, (b) Thresholding to highlight only the pixels with highest intensity, (c) Column scanning to highlight the posterior surface of the vertebrae and (d) Applying the transformation of Equation 3 to compute each point in the Polaris COS.

Registration

After acquiring the preoperative and intraoperative images of the lumbar spine, the data derived from the two imaging modalities must be merged, through finding the transformation between the CT COS and the Polaris COS. The registration is the central piece of any image-guided (IG) procedure and allows to compute the preoperative surgical plans in the

intraoperative COS, guiding the surgeon to the desired trajectories.

In this project, as our objective was to match a US-derived Point Cloud (PC) with a CT-derived PC, we used a combination of active registration methods, the pair-points and surface matching. The first step of our registration methodology was to manually identify a set of vertebral landmarks (fiducials) in the two types of correspondent PC, which were matched using Kabsch algorithm. The result of this step was then used as the initial estimation to perform the surface matching step, for which we used the Iterative Closest Point (ICP) algorithm. All the registration process was computed using MATLAB®.

Kabsch Algorithm

Proposed in 1976 by Wolfgang Kabsch [15], the algorithm commonly known by the name of its author consists in a method for finding the transformation which best relates two sets of vectors. To apply this algorithm there must be correspondence between each vector from the first set with each vector from the second set. Since there is correspondence between each vector set, the translation part of the transformation comes down to the difference between their centroids, leaving only the rotation part to be computed.

Being P and Q two sets of vectors, represented as $N \times 3$ matrices, where each row corresponds to the coordinates of each vector in \mathbb{R}^3 , the steps for computing the rotation matrix which rotates P into Q are calculating the cross-covariance matrix H (7), calculating the singular value decomposition (SVD) of H (8) and computing the rotation matrix R (9).

$$H = P^T Q \quad (7)$$

$$H = USV^T \quad (8)$$

$$R = V \begin{bmatrix} 1 & 0 & 0 \\ 0 & 1 & 0 \\ 0 & 0 & \det(VU^T) \end{bmatrix} U^T \quad (9)$$

ICP Algorithm

Unlike Kabsch algorithm, the ICP algorithm, introduced in 1992 by Paul Besl and Neil McKay [16], is employed to relate two sets of points without the need of a correspondence between each point, which means that the two data sets may not even have the same number of points. ICP computes the transformation which best relates two PC by iteratively minimizing the root mean square of the metric distance between the points of the two data sets. ICP usually converges to a local minimum which may not correspond to the ideal transformation that align one PC to another, so it is very important to give the algorithm a good initial transformation.

Being Q a fixed PC with M points – $Q = \{\vec{q}_1, \vec{q}_2, \dots, \vec{q}_M\}$, $\vec{q}_m \in \mathbb{R}^3$ – commonly known as reference, and P another PC with N points – $P = \{\vec{p}_1, \vec{p}_2, \dots, \vec{p}_N\}$, $\vec{p}_n \in \mathbb{R}^3$ – known as source, that must be transformed to best match the reference, the steps for computing the transformation matrix which aligns P into Q are calculating for each point of P the closest point in Q , matching each (\vec{p}_n) with its closest (\vec{q}_m) , the transformation

T – combination of a 3x3 rotation matrix R and a translation vector \vec{t} – which minimizes the sum of the squared distance between each pair of matching points (10) using a Least Squares approach, transform the source data set P with the computed transformation T (11), verify the stopping criteria, namely the number of iterations or differences between consecutive iterations and repeat if stopping criteria was not met.

$$\min \sum_{n=1}^N |R * \vec{p}_n + \vec{t} - \vec{q}_m|^2 \quad (10)$$

$$P_{i+1} = T_i P_i = R_i P_i + \vec{t}_i \quad (11)$$

The result of the registration process is the transformation $T_{Polaris}^{CT}$, which sets the correspondence between the CT COS and the Polaris COS

$$T_{Polaris}^{CT} = T_{CT^*}^{CT} * T_{Polaris}^{CT^*} \quad (12)$$

where $T_{Polaris}^{CT^*}$ results from applying Kabsch algorithm and $T_{CT^*}^{CT}$ results from the ICP algorithm refinement.

Navigation System

The navigation system is the culmination of the presented work, where all the gathered data and the computed transformations are merged to display real-time visual guidance to the surgeon who is performing the insertion of the pedicle screws.

The navigation system created for this project is a simple MATLAB® graphical user interface (GUI), which allows to display the lumbar spine, the surgical plans and the Polaris tools in the intraoperative COS – the Polaris COS. For this, it receives as inputs the CT-derived PC, the surgical plans performed in the CT COS, which include the insertion points and orientations for every pedicle screw we want to place, and the transformation matrix from the Polaris COS to the CT COS – $T_{Polaris}^{CT}$, as computed in the registration process.

After loading these data, it computes the transformation matrix from the CT COS and the Polaris COS, for displaying the CT-derived PC and the surgical plans in the Polaris COS. This transformation is the inverse of the matrix which transforms from the Polaris COS to the CT COS,

$$T_{CT}^{Polaris} = (T_{Polaris}^{CT})^{-1} \quad (13)$$

To assist the surgery, each pedicle screw plan is exhibited as a red cone with the vertex in its insertion point. The cone's axis of symmetry is aligned with the planned orientation vector. Then, it is possible to initialize the real-time visualization of the surgical tools. The navigation system communicates with the Polaris system and gets the information about the tools positions and orientations. Although it is possible to track any instrument that has a group of Polaris markers attached, the presented navigation system only tracks the Polaris pointer.

When the connection with the Polaris system is achieved, the navigation system displays in real-time the pointer's position and orientation in the Polaris COS. The pointer

referential is exhibited as a red dot and the pointer itself is a blue line. To help the surgeon reach the desired pedicle screw's placement, each one of the cones of the surgical plans turn from red to green when the Polaris pointer's tip is inside the correspondent cone and it is aligned with its axis of symmetry.

5. Results

CT scan, CT model and surgical planning

The segmentation of the phantom CT-scan resulted in seven 3D models, corresponding to the vertebrae T11, T12, L1, L2, L3, L4 and L5, which are presented in Figure 9.

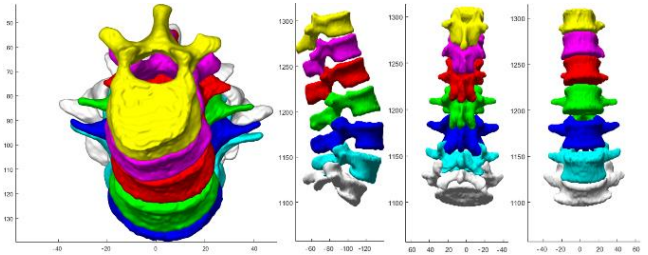


Figure 9 - Superior, lateral (right), posterior and anterior view of the seven vertebrae 3-D modes.

The coordinates of the insertion points and the directions, given by unit vectors, which were planned for each screw of the L2, L3 and L4 vertebrae, in the COS of the CT-scan, are presented in Table 1.

Table 1 - Coordinates of the insertion points and directions for the planned pedicle screws.

	Insertion Point (mm)	Direction
LEFT		
L2	(20.41 , -82.97 , 1206.07)	(-0.236 , -0.924 , 0.300)
L3	(23.26 , -90.38 , 1181.07)	(-0.266 , -0.964 , 0)
L4	(25.54 , -89.81 , 1153.07)	(-0.293 , -0.939 , -0.179)
RIGHT		
L2	(-13.22 , -81.26 , 1207.07)	(0.213 , -0.943 , 0.257)
L3	(-14.93 , -89.24 , 1178.07)	(0.248 , -0.969 , 0)
L4	(-17.21 , -88.67 , 1150.07)	(0.261 , -0.963 , -0.061)

The results of the CT-derived PC containing the posterior regions of the lumbar spine are presented in Figure 10.

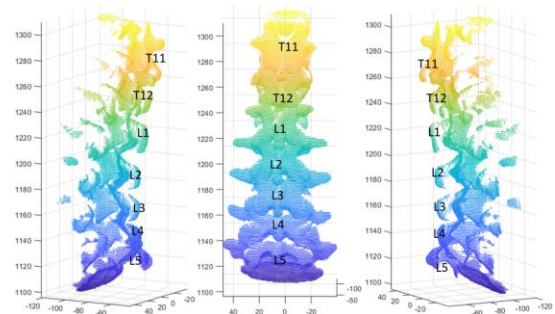


Figure 10 - Point Cloud of the posteriormost regions of all the vertebrae.

The CT-derived PC used for registration were the PC shown in the previous figure (for register with the US data acquired of the full length of the phantom) and a sub-group of

it, which included only the points of the L3 vertebra (for register with the US data acquired only at the L3 level).

Freehand 3-D Ultrasound imaging

The results of the tip position, in the Pointer ROS and the respective error of the best pointer tip calibration were, respectively, $(-17.27, 1.07, -157.30)$ (mm) and 0.37 mm.

The results of probe calibration parameters - $s_u, s_v, t_x, t_y, t_z, \alpha, \beta$ and γ -, the error in each coordinate axis and the RMSE for the best probe calibration were, respectively, 0.126 mm/pixel, 0.120 mm/pixel, $(-34.19, -21.06, -36.62)$ (mm), $-91.70^\circ, -43.34^\circ, 268.28^\circ$, $(0.23, 0.31, 0.65)$ (mm) and 0.44 (mm).

All the probe calibration process was performed with US image depth of 50 mm. Figure 11 shows a qualitative result of the best probe calibration achieved, where Stradwin was able to identify the pointer's tip purely based on the Polaris data and the probe calibration, without any kind of tip segmentation.

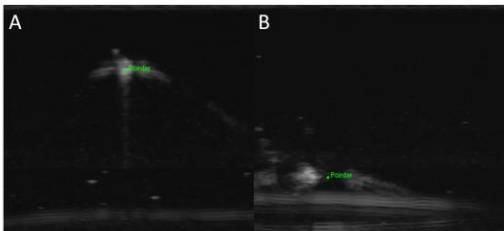


Figure 11 - Calibration result. In this figure, the pointer's tip is identified based on the Polaris data and not based on image segmentation. A: Tip close to US probe. B: Tip far from the US probe.

After calibration we acquired five US volumes, which were segmented, resulting in the five US-derived PC depicted in Figure 12 and Figure 13.

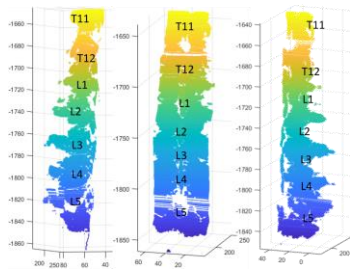


Figure 12 - US-derived PC resulting from the segmentation of the full lumbar spine – medial, left and right US acquisitions, in the Polaris COS.

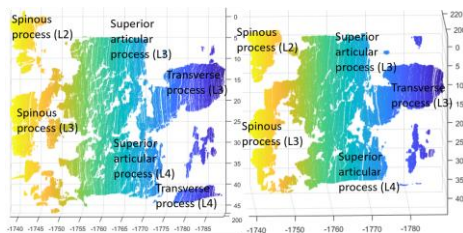


Figure 13 - US-derived PC resulting from the segmentation of the L3 vertebra – right (1st and 2nd) US acquisitions, in the Polaris COS.

Registration

After performing the segmentation of the US volumes, obtaining the different US-derived PC, these sets of points were merged with the CT-derived data using the presented registration methods. We started by select three fiducials in each Point Cloud pair to run the Kabsch algorithm, then run the ICP algorithm using the CT-derived PC as reference and each US-derived PC after the initial approximation as source. The results of the registration step and their RMSE are shown in Figure 15 to Figure 33. The US-derived PC of the L3 vertebra were registered initially with only the CT-derived L3 PC, to perform registration of single vertebra, and after with the CT-derived full PC, which presented better results, presented in FIGURES.

Navigation System

Figure 14 shows the navigation system interface with the pointer's tip in the planned insertion point for the L2 left pedicle screw (A) and the Pointer in that position relative to the lumbar spine phantom (B and C).

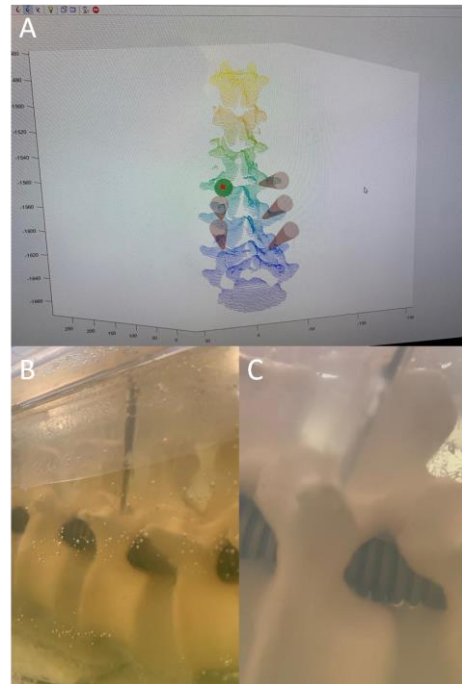


Figure 14 - Polaris Pointer surgical plan for left L2 pedicle screw. A: Navigation System. B and C: Lumbar Spine Phantom.

6. Discussion

CT-scan

In the CT-data acquired, it was possible to differentiate all the interesting regions of the lumbar phantom, since there was a good contrast between the image intensity of the different materials. However, it is important to note that this data presents some differences when faced against the CT-data of a real human subject.

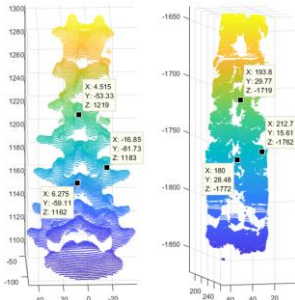


Figure 15 - Selection of the pair-points in CT-derived PC and in the full lumbar spine – medial US PC.

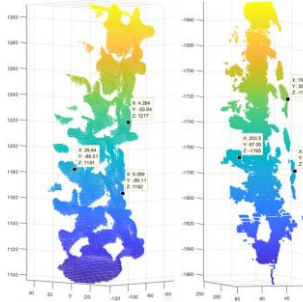


Figure 18 - Selection of the pair-points in CT-derived PC and in the full lumbar spine – left US PC.

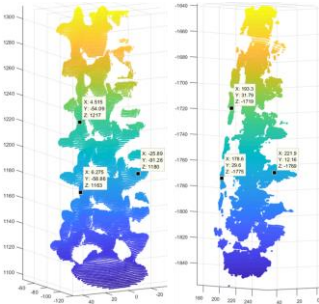


Figure 21 - Selection of the pair-points in CT-derived PC and in the full lumbar spine – right US PC.

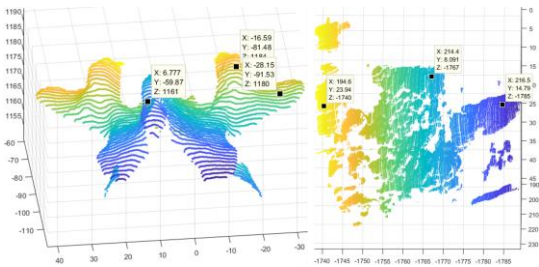


Figure 24 - Selection of the pair-points in CT-derived L3 PC and in the L3 vertebra – right (1st) US PC.

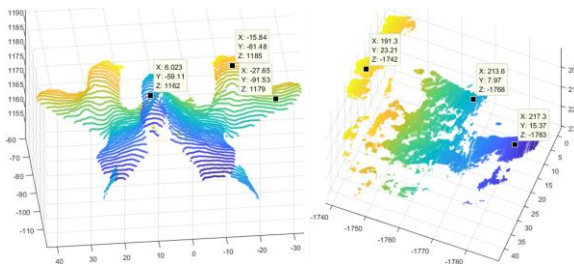


Figure 27 - Selection of the pair-points in CT-derived L3 PC and in the full lumbar spine – medial US PC.

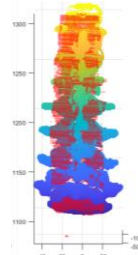


Figure 16 - Result of Kabsch algorithm for the first US acquisition (in red). RMSE = 0.9982 mm

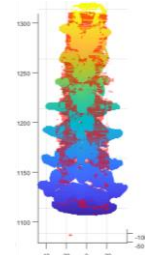


Figure 17 - Result of the ICP algorithm for the first US acquisition (in red). RMSE = 2.2067 mm

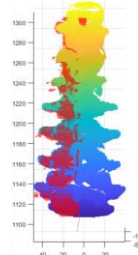


Figure 19 - Result of Kabsch algorithm for the second US acquisition (in red). RMSE = 2.2104 mm

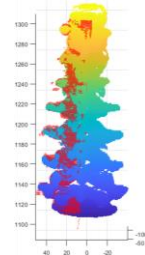


Figure 20 - Result of the ICP algorithm for the second US acquisition (in red). RMSE = 1.9867 mm

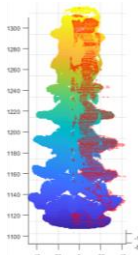


Figure 22 - Result of Kabsch algorithm for the third US acquisition (in red). RMSE = 1.5392 mm

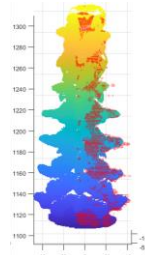


Figure 23 - Result of the ICP algorithm for the third US acquisition (in red). RMSE = 1.9175 mm

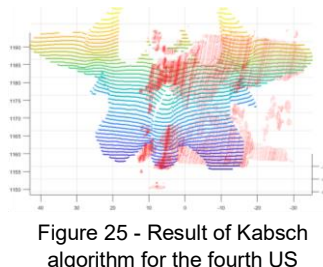


Figure 25 - Result of Kabsch algorithm for the fourth US acquisition (in red). RMSE 1.4931 mm

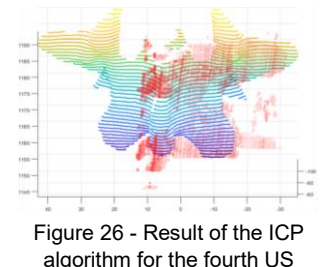


Figure 26 - Result of the ICP algorithm for the fourth US acquisition (in red). RMSE 5.2870 mm

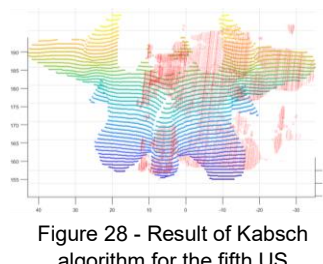


Figure 28 - Result of Kabsch algorithm for the fifth US acquisition (in red). RMSE = 0.5853 mm

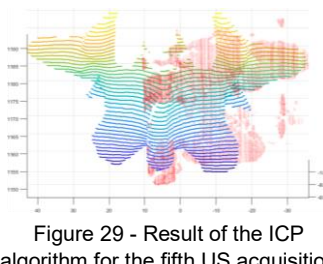


Figure 29 - Result of the ICP algorithm for the fifth US acquisition (in red). RMSE = 2.5279 mm

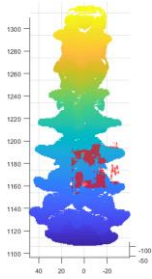


Figure 30 - Result of the ICP algorithm for the fourth US acquisition (in red) with all vertebrae. RMSE 2.5279 mm

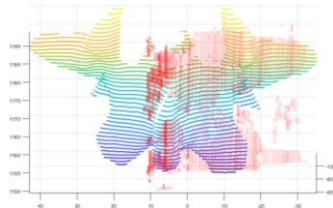


Figure 31 – Detail of Figure 30.

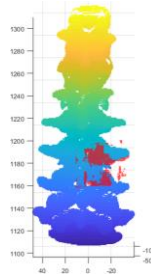


Figure 32 - Result of the ICP algorithm for the fifth US acquisition (in red) with all vertebrae. RMSE 2.6175 mm

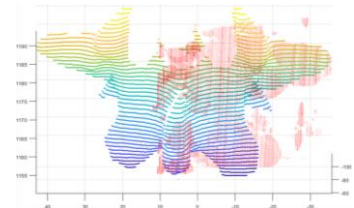


Figure 33 – Detail of Figure 32.

Through this CT-scan we were able to obtain a very good CT-derived 3-D model of our phantom. Evaluating qualitatively, we consider that the segmentation performed was able to highlight all the phantom features, with the resulting vertebral models (T11, T12, L1, L2, L3, L4 and L5) being almost identical to the printed models that gave them origin. Also, through the CT-data and the CT-derived 3-D models, it was possible to successfully plan the insertion points for the pedicle screws at the L2, L3 and L4 level and their ideal directions, using the MATLAB® GUI created for this task and according to medical guidance.

Freehand 3-D Ultrasound imaging

The key step in Freehand 3-D Ultrasound imaging is the probe calibration. It is this step that allows to accurately acquire an intraoperative US-volume, by computing the real intraoperative location of a multiple set of US frames and of the internal features captured in them. The calibration method chosen made use of the Polaris pointer to set the parameters constrains to calculate the transformation between the US probe and the US frame, and so, the first step in the calibration process was to calibrate the Polaris pointer.

This calibration step proved to be quick, simple and accurate, with an error lower than 0.5 mm.

Probe calibration proved to be more complex, difficult and user-dependent than the previous one, mainly due to the difficulty in correctly aligning the tip of the pointer with the US frame and accept the tip segmentation at the same time. Although this process presented a RMSE of around 0.5 mm, we could notice a difference in the convergence between the upper part of the US frame, which stands closer to the US probe, and the bottom part of the image. This problem, which can be verified in Figure 11, results from the fact that the image of the pointer's tip in the US B-mode is more perceptible if the pointer is perpendicular to the direction of the US waves, near the water bath surface.

The acquired US volumes were computed in the Polaris COS correctly after the calibration was performed. The US frames acquired by scanning the surface of the lumbar phantom allowed to differentiate the key features of the posterior regions of each vertebra, mainly their spinous and

transverse processes. Their articular processes and their laminae could also be seen but were not so easily differentiated. This could be seen after segmentation, shown in Figure 12 and Figure 13. Comparing with the CT data, we could conclude that US imaging is noisier and presents fewer perceptible details.

In the US acquisitions of the L3 vertebra – right, we were unable to scan only that vertebra, resulting in the inclusion of regions of the adjacent vertebrae, which had implications in registration.

Registration

Kabsch algorithm allows to compute the transformation between two sets of matching points. This algorithm proved to be simple and useful to calculate the initial approximation between the different PC, although it was very user dependent for the fiducial selection. Despite this, we achieved good results applying Kabsch algorithm, with RMSE of the fiducials of around 2 mm.

ICP algorithm was used to refine the already good approximation between the CT and US-derived PC. Although ICP iteratively minimized the mean distance between the points of the US-derived PC and the CT-derived PC to around 2 mm, comparing Figure 16 with Figure 17, Figure 19 with Figure 20 and Figure 22 Figure 23, one could not notice many improvements. The presented error measurement evaluates the mean distance between the different PC after registration, known as Registration Error (RE). To completely evaluate the registration process, we would need to measure another type of error, which considers the difference in the position and orientations of specific targets of the lumbar phantom, known as the Target Registration Error (TRE). We decided to don't measure the TRE because we would need to insert the Polaris pointer in the gelatine several times, which would damage the phantom, increasing the noise of the acquired US data.

The results of applying ICP to the L3 vertebra – right US PC using only the L3 CT-derived PC present a great error. This shows that this method could not be used to perform registration when the source PC includes regions which are not present in the reference PC. Using the complete CT-

derived PC allowed to achieve better results, similar to the ones with the full lumbar spine US PC.

Navigation System

Our navigation system was created with the objective of presenting the potential of the developed work. With this navigation system we were able to correctly track the Polaris pointer and visually control its position relative to the lumbar spine and the surgical plans. The results presented in Figure 14 allow to see a good match between the position of the Polaris pointer in the navigation system and in the real lumbar spine phantom. This was possible due to the good results presented in the registration step.

There is some error associated with this method, that arises from the accumulation of errors of each individual step, mainly the Pointer Pivoting, the Probe Calibration and the Registration processes. However, using the Navigation System we were not able to numerically quantify the existing error, mainly due to the absence of targets in the lumbar spine phantom that would allow to evaluate TRE, as explained in the previous subsection.

Although we could not present more quantitative results, this system allows to draw some important qualitative conclusions regarding the performed procedure.

7. Conclusion

The goal of this project was to simulate an image-guided surgery for inserting pedicle screws in the lumbar spine, using Freehand 3-D Ultrasound imaging as the intraoperative imaging modality and performing registration between the preoperative CT data and the intraoperative data. Although there was no actual pedicle screw placement, it is possible to affirm that we managed to achieve this goal, since the preoperative and intraoperative work necessary to carry this kind of image-guided procedure was concluded. Despite some limitations in the registration process, which arise mainly from the poor detail of US-data acquired, we could affirm that US can be used as intraoperative image modality to assist image-guided surgeries for pedicle screw placement. The overall results are optimistic for a laboratory practice, however, for a clinical practice, they lack quantification of the total error associated with registration process, combining RE and TRE. To overcome this aspects, further studies are needed.

Acknowledgements: This document was written and made publicly available as an institutional academic requirement and as a part of the evaluation of the MSc thesis in Biomedical Engineering of the author at Instituto Superior Técnico. The work described herein performed at the Surgical Robotics Lab (SRL) of IDMEC, Instituto Superior Técnico (Lisbon, Portugal), during the period February 2018 May 2019, under the supervision of Prof. Jorge Martins from IST and the

co supervision of Dr. Manuel Herculano from Hospital de Santa Maria.

References

- [1] T. Vos *et al.*, "Years lived with disability (YLDs) for 1160 sequelae of 289 diseases and injuries 1990–2010: a systematic analysis for the Global Burden of Disease Study 2010," *Lancet*, vol. 380, no. 9859, pp. 2163–2196, Dec. 2012.
- [2] J. Pelozza, "Surgery for Lower Back Pain." [Online]. Available: <https://www.spine-health.com/conditions/lower-back-pain/surgery-lower-back-pain>.
- [3] J. McCormick, M. Aebi, D. Toby, and V. Arlet, "Pedicule screw instrumentation and spinal deformities: have we gone too far?," *Eur. Spine J.*, vol. 22 Suppl 2, pp. S216–24, Mar. 2013.
- [4] G. L. Lowery and S. S. Kulkarni, "Posterior percutaneous spine instrumentation," *Eur. Spine J.*, vol. 9, no. S1, pp. S126–S130, 2000.
- [5] K. T. Foley and S. K. Gupta, "Percutaneous pedicle screw fixation of the lumbar spine: preliminary clinical results.," *J. Neurosurg.*, vol. 97, no. 1 Suppl, pp. 7–12, Jul. 2002.
- [6] L. Khoo, "Rationale for minimally invasive spine surgery," in *An anatomic approach to Minimally Invasive Spine Surgery*, M. Perez-Cruet, Ed. St.Louis, Missouri: Quality Medical Publishing Inc., 2006, pp. 89–102.
- [7] L.-P. Nolte, H. Visarius, E. Arm, F. Langlotz, O. Schwarzenbach, and L. Zamorano, "Computer-aided fixation of spinal implants," *J. Image Guid. Surg.*, vol. 1, no. 2, pp. 88–93, 1995.
- [8] D. Rixen *et al.*, "Image-guided spine surgery: state of the art and future directions," *Eur. Spine J.*, vol. 19, no. 1, pp. 25–45, 2009.
- [9] T. Ungi, E. Moulton, J. H. Schwab, and G. Fichtinger, "Tracked ultrasound snapshots in percutaneous pedicle screw placement navigation: a feasibility study.," *Clin. Orthop. Relat. Res.*, vol. 471, no. 12, pp. 4047–55, Dec. 2013.
- [10] B. Brendel, S. Winter, A. Rick, M. Stockheim, and H. Ermert, "Registration of 3D CT and ultrasound datasets of the spine using bone structures.," *Comput. Aided Surg.*, vol. 7, no. 3, pp. 146–55, 2002.
- [11] NDI Medical, "Polaris Spectra and Vicra." [Online]. Available: <https://www.ndigital.com/medical/products/polaris-family/>. [Accessed: 28-Mar-2019].
- [12] G. Treece, A. Gee, and R. Prager, "Stradwin." [Online]. Available: <http://mi.eng.cam.ac.uk/~rwp/stradwin/docs/intro.htm>. [Accessed: 28-Mar-2019].
- [13] P.-W. Hsu, G. M. Treece, R. W. Prager, N. E. Houghton, and A. H. Gee, "Comparison of Freehand 3-D Ultrasound Calibration Techniques Using a Stylus," *Ultrasound Med. Biol.*, vol. 34, no. 10, pp. 1610–1621, Oct. 2008.
- [14] J. J. Moré, "The Levenberg-Marquardt algorithm: Implementation and theory," in *Numerical Analysis (Lecture Notes in Mathematics)*, Springer-Verlag, 1977, pp. 105–116.
- [15] W. Kabsch, "A solution for the best rotation to relate two sets of vectors," *Acta Crystallogr. Sect. A*, vol. 32, no. 5, pp. 922–923, Sep. 1976.
- [16] P. J. Besl and N. D. McKay, "A method for registration of 3-D shapes," *IEEE Trans. Pattern Anal. Mach. Intell.*, vol. 14, no. 2, pp. 239–256, Feb. 1992.